Design, Hemiysnthesis, crystal structure and anticancer activity of 1, 2, 3-triazoles derivatives of totarol

Yassine Laamari, Ali Oubella, Abdoullah Bimoussa, Az-Eddine El Mansouri, El Mostafa Ketatni, Olivier Mentré, My Youssef Ait Itto, Hamid Morjani, Mostafa Khouili, Aziz Auhmani

Design, Hemiysnthesis, crystal structure and anticancer activity of 1, 2, 3-triazoles derivatives of totarol

Yassine Laamari [a] , Ali Oubella [a] , Abdoullah Bimoussa [a] , Az-Eddine El Mansouri [e] , El Mostafa Ketatni [b] , Olivier Mentre [c] , My Youssef Ait Itto [a] , Hamid Morjani [d] , Mostafa Khouili [b] , Aziz Auhmani [a,*]

a Laboratoire de Synthése Organique et Physico-Chimie Mol´eculaire, Département de Chimie, Faculté des Sciences, Semlalia, Universit´e Cadi-Ayyad, B.P 2390, Marrakech 40001, Morocco

b Laboratory of Applied Spectro-Chemistry and the Environment, 10 University Sultan Moulay Slimane, Faculty of Sciences and Technology, PO Box 523, Beni-Mellal, Morocco

c Univ. Lille, CNRS, Centrale Lille, ENSCL, Univ. Artois, UMR 8181 - UCCS-Catalysis and Solid Chemistry Unit, F-59000 Lille, France

d BioSpectroscopieTranslationnelle, BioSpecT – EA7506, UFR de Pharmacie, Universit´e de Reims Champagne-Ardenne, 51 Rue Cognacq Jay, 51096 Reims Cedex, France

e Laboratory of Biomolecular and Medicinal Chemistry, Department of Chemistry, Faculty of Science Semlalia, BP 2390, Marrakech 40001, Morocco

Abstract

A new series of diverse triazoles linked to the hydroxyl group of totarol were synthesized using click chemistry approach. The structure of these compounds was elucidated by HRMS, IR and NMR spectroscopy. The structure of compound **3g** was also confirmed by x-ray single crystal diffraction. The cytotoxicity of these compounds was evaluated by the MTT method against four cancer cell lines, including fibrosarcoma HT-1080, lung carcinoma A-549, and breast adenocarcinoma (MDA-MB-231 and MCF-7), and the results indicated that all compounds showed weak to moderate activities against all cancer cell lines **,**with IC_{50} values ranging from 14.44 to 46.25 μM. On the basis of our research the structure-activity relationships (SAR) of these compounds were discussed. This work provides some important hints for further structural modification of totarol towards developing novel and highly effective anticancer drugs. Respectively. It is interesting to note that the compound **3g** indicated a very significant cytotoxicity against HT-1080 and A-549 cell lines.

Keywords: 1,2,3-triazole–totarol hybrids, crystal structure, Hirshfeld surface analysis, cytotoxicity activity, Apoptosis, Cell cycle

Introduction

Cancer is the major deadly and feared disease worldwide [**1**]. caused by a chronic, uncontrolled, and pathological proliferation of anormalous cells. These abnormal cells can

square circulations, and harm organ capacities which may lead to death [**2**]. Cancer, being a superb burden to both the society and single human lives. In spite of the fact that there have been advances within the improvement of treatment and avoidance of cancer, the victory to treat cancer remains a challenge [**3**]. Consequently, there is still an urgent need to search for novel anticancer dealers that have broader spectrum of cytotoxicity to tumor

Natural products contribute appreciably in the anticancer drug discovery system by serving as important leads for the development of novel treatments [**4-5**]. Totarol (**I**) is a naturally occurring phenolic diterpene isolated from severa plants of the Podocarpaceae and Cupressaceae families and has been reported to exhibit important pharmacological activities including antifungal activities [**6**], antimalarial [**7**], antibacterial [**8**] and antiplasmodial activity [**9**]. Furthermore, current research have shown that totarol, induced selective cytotoxic effects in SGC-7901 human gastric cancer cells by inducing apoptosis cell cycle arrest and inhibition of cell migration [**10**]. Besides, S. Mahdjour and cowerkers reported that totarol derivatives such as catechol (**II**) (Fig. 1) and *ortho*-quinone (**III**) (Fig. 1) had marked antiproliferative activities against MCF-7, T-84, and A-549 cell lines [**11**]. Moreover, ferruginol (**IV**) (Fig. 1) is a totarol isomer that showed significantly suppresses the proliferation through apoptosis-mediated cell death as caspase-3 activator [**12**].

On the other hand, 1,2,3-Triazole derivatives have attracted the attention of medicinal chemists due to their wide biological profiles such as antibacterial [**13**], antitubercular [**14**], antimalarial [**15**], antifungal [**16**], antiviral [**17**]. In particular, 1,4-disubstituted 1,2,3-triazoles can be used to exhibit significant antiproliferative action against a wide range of human cancer cell lines [**18**]. Recently, Yong-Cheng et al., reported a newly hybrids of triazole and Jaridonin (**V**) (Fig. 1), which showed potent antitumor activity against HGC-27 and MGC-803 cells through inducing apoptosis and cell cycle arrest [**18**]. Also, 1,2,3-triazole hybrid (**VI**)(Fig. 1) exhibited remarkable anticancer activity against MCF-7 (IC_{50} = 0.38 µM) and MDA-MB-231 (IC_{50} = 0.48 µM) cell lines [**19**]. In addition compound (**VII)** (Fig. 1) proved a highly strong cytotoxicity even at submicromolar concentrations, against various cancer cell lines such as DLD-1, B16, Hela, SiHa, A172, and. U-87 [**20**]. Similarly compound (**VIII)** (Fig. 1) showed cytotoxic activity with an IC_{50} value of 0.8 µM against SMMC-7721 cells relative to cisplatin as a reference drug [**21**].

Were designed by the incorporation of the totarol and 1,2,3-triazole via methylene linker to combine the benefits of their effects to give a compact structure with promising anticancer activity. The methyl bridge has chosen due to his greater flexibility around a CH_2–triazole moiety. Also, to study the structure-activity relationship, various phenyl and alkyl derivatives were introduced to the triazole ring. The target compounds were evaluated against

four human cancer cell lines including, fibrosarcoma (HT-1080), lung carcinoma (A-549), and breast adenocarcinoma (MDA-MB-231 and MCF-7) using the MTT assay. Then, the possible mechanism of apoptosis induction was studied using apoptosis through caspase-3/7 activation and cell-cycle arrest in HT-1080 and A-549.

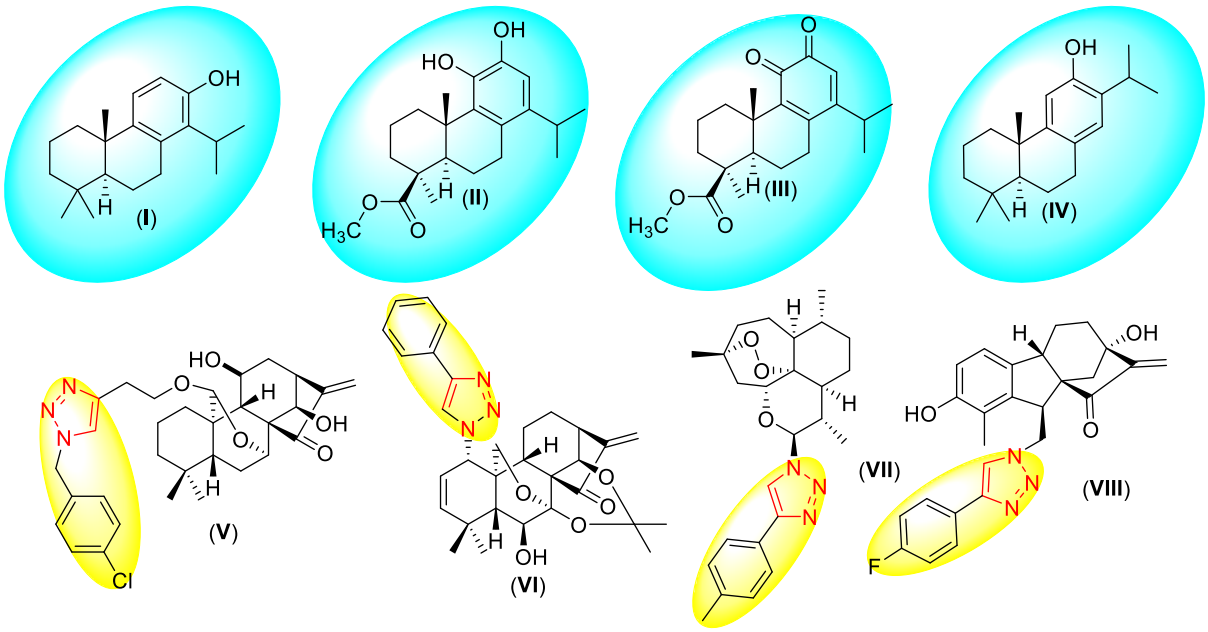

Fig. 1. Structures of compounds **I-VIII.**

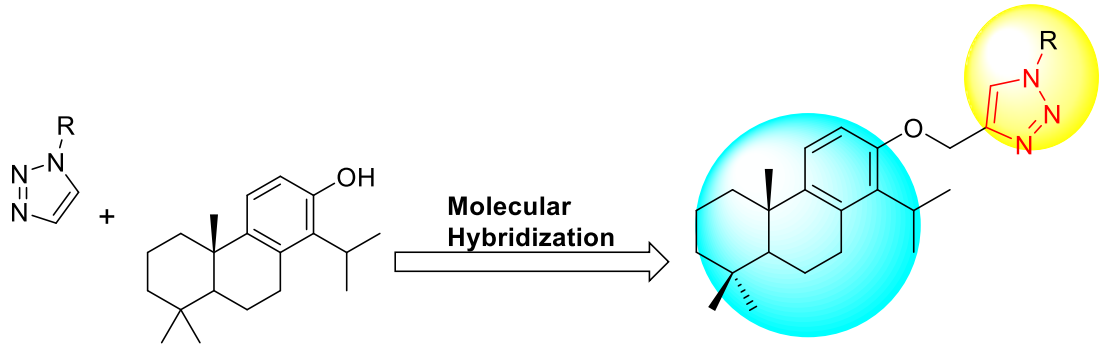

Fig. 2. Pharmacophore of the target compounds.analogues

Results and discussion

The “Click” chemistry is a powerful, reliable, and highly selective technique for the efficient and rapid synthesis of large varieties of structures compounds [19]. Recent reports show that click chemistry of natural products is a very useful tool for the development of bioactive natural product analogs [**20**]. Of the reactions comprising the click world, the ideal

example is the copper-catalyzed 1,3-dipolar azide-alkyne cycloaddition (CuAAC) reaction [21] to form 1,4-disubstituted-1,2,3-triazoles.

The naturally occurring diterpenoid totarol (**I**) was isolated from dichloromethane extract of the wood of *Tetraclinis articulata* by flash chromatography using silica gel as stationary phase and hexane as eluent. the compound was identified by spectroscopic methods and was used for chemical modifications in the present work.

First, totarol was subjected propargylation at the only hydroxyl group with propargyl bromide in presence of potassium carbonate in acetone affording an O-tethered terminal alkyne (**2**). The structure of this intermediate was elucidated from its IR and NMR spectral data. In the IR spectrum, the presence of the propargyl ether is evidenced by the bands at 3311 and 2132 cm^{-1} related to the stretching of the terminal alkyne C–H bond and to the C≡C bond, respectively; an intense band at 1046 cm^{-1} corresponding to the stretching of the C–O ether bond was too observed. Moreover, its ^{1}H NMR spectrum showed especially the disappearance of the hydroxyl peak at 4.52 . ppm, and the appearance of signals for the propargyl moiety at 4.78 and 2.58 ppm relative to H-3' and H-1', respectively. Characteristic signals in the ^{13}C NMR spectrum were showed at δ 74.8, 55.5 and 50.5 ppm attributed to the propargylic carbons C-2', C-1' and C-3' respectively.

Azides were synthesized by two methods first, aromatic azides were prepared by Sandmeyer-type reactions, as shown in Scheme 1. each one of the different aromatic amines was treated with sodium nitrite supported on the surface of silica sulfuric acid. at low temperature (0 to 5 ºC), generating its respective aryldiazonium silica sulfates that were simultaneously converted to the respective azide by addition of sodium azide to the reaction mixture.in other hand the alkyl azides were prepared from the corresponding organic bromides by stirring the bromide with NaN_3 in water/acetone (1:3) at room temperature to give the desired azide as yellow oil. The different azide moieties were further used in convergent synthetic approaches, as shown in Scheme 2.

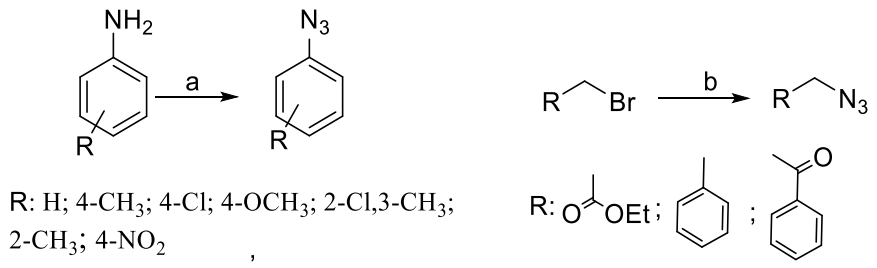

Scheme 1. Synthetic route for azides compounds. Reagents and conditions: (**a**) i-$NaNO_2$, silica sulfuric acid, ii-NaN_3 ,H_2O 0 °C to rt, 2 hr; (**b**) NaN3, Acetone-H_2O (3:1), rt, 24 hrs.

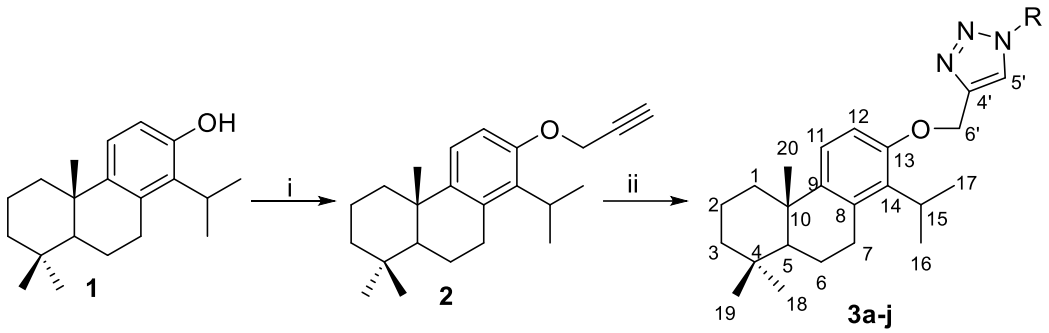

Compd.	a	b	c	d	e	f	g	h	i	j
R	Phenyl	4-Tolyl	4-Chlorophenyl	4-Methoxyphenyl	3-Chloro-2-methylphenyl	2-Tolyl	4-Nitrophenyl	Ethyl acetyl	Benzyl	phenacyl

Scheme 2. Synthetic route for target compounds **3a-j**. Reagents and conditions: (**i**) Propargyl bromide, K_2CO_3, Acetone, 24 hr; (**ii**) appropriate azide, $CuSO_4 \cdot 5H_2O$, sodium ascorbate, E*t*OH:H_2O 1:1

The approach used for the synthesis of 1,2,3-triazole-totarol hybrids **3a-j** (Scheme 2) is referred by Rostovtsev *et al*. [**22**]. The terminal alkyne **2** was treated with the appropriate azide in the presence of copper sulfate and sodium ascorbate, the metal is reduced *in situ* and the cycloaddition reaction takes place. The solvent used in this kind of reaction is a system composed of ethanol and water (1:1) that is stirred at room temperature while the development of the reaction is monitored by TLC .At the end, the triazoles are isolated and purified by silica column chromatography. The products were obtained with yields ranging from 70 to 84%.The ^{1}H NMR spectra of the click reaction products **3a-j** revealed the appearance of the new signals of the incorporated aryl groups at δ 6.8-7.9 ppm compared with the spectra of the starting terminal alkyne **2** , while the H-triazole singlet was identified at δ 7.7-8.2 ppm. Compound **3h** containing an alkyl substituent was an exception, with a chemical shift of 7.79 ppm (H-triazole) and signals at δ 5.1-5.6 ppm for OCH_2, in addition to signals corresponding to the totarol moiety hydrogens. Thus, at δ 0.90-1.4 ppm three singlets at 0.93,0.99 and 1.30 ppm were observed corresponding to H-19, H-18 and H-20 methyl, and two doublets at δ 6.74 and 7.14 ppm, relative to the hydrogens H-12 and H-11 respectively.

Crystal structure of 2 and 3g

The crystal structures determination details of both compounds **2** and **3g** are given in Table 1, selected bond lengths and angles given in Table 2. For both compounds, the crystal structures were determined in monoclinic and triclinic symmetry, where the **2** and **3g** crystallize in the non centrosymmetric space groups $P2_1$ *c* and *P*1, respectively.

The structure is built up from three fused six- membered related to prop-2-yn-1-yloxy for **2** and to (4-nitrophenyl)-1H-1,2,3-triazole for **3g (Fig. 3)**. In both molecules, there are two chiral carbon atoms, C5 exhibits an S configuration and C10 exhibits an S configuration.

Table 1 Crystal Data, Summary of Intensity Data Collection, and Structure Refinement

	2	**3g**
Empirical formula	$C_{23}H_{32}O$	$C_{29}H_{36}N_4O_3$
Formula weight	324.48	488.62
Temperature	298(2)	298(2)
Wavelength	0.71073 Å	0.71073 Å
Crystal system, space group	Monoclinic, $P2_1$	Triclinic, *P*1
a, b, c (Å)	6.0943(18), 22.019(8), 7.491(2)	6.0325(18) , 10.887(3), 10.925(3)
α, β, γ (°)	90, 107.94(2), 90	115.143(15), 92.018(16), 97.678(17)
Volume (A^3)	956.3(5)	640.3(3)
Z	2	1
Calculated density (g/cm^3)	1.127	1.267
μ (mm^{-1})	0.066	0.083
Crystal size (mm)	0.40x0.31x0.11	0.45x0.29x0.19
Theta range for data collection (°)	2.858 - 24.986	2.070 - 24.999
Limiting indices	-7 ≤h ≤7, -21 ≤ k ≤25, -8 ≤ l≤ 8	-7 ≤h ≤7, -12 ≤ k ≤12, -12 ≤ l≤ 12
Diffractometer	Bruker DUO APEXII CCD diffractometer	Bruker DUO APEXII CCD diffractometer
Absorption correction	Multi-scan (*SADABS*, Brucker, 2012)	Multi-scan (*SADABS*, Brucker, 2012)
Tmin. Tmax.	0.6541 - 0.7469	0.6039 - 0.7456
No. of measured, independent and observed [$I > 2\sigma(I)$] reflections	10611, 2940, 2474 [R(int) = 0.030]	12563, 4215, 2430 [R(int) = 0.055]
Refinement method	Full-matrix least-squares on F^2	Full-matrix least-squares on F^2
Data / restraints / parameters	2940/1/222	4215/3/344
R[$F^2 > 2\sigma(F^2)$], wR(F^2), S	0.041; 0.101, 1.05	0.051, 0.132, 0.94
H-atom treatment	H-atom parameters constrained	H atoms treated by a mixture of independent and constrained refinement
$\Delta\rho_{max}$, $\Delta\rho_{min}$ (e $Å^{-3}$)	0.14, −0.16	0.15, −0.13

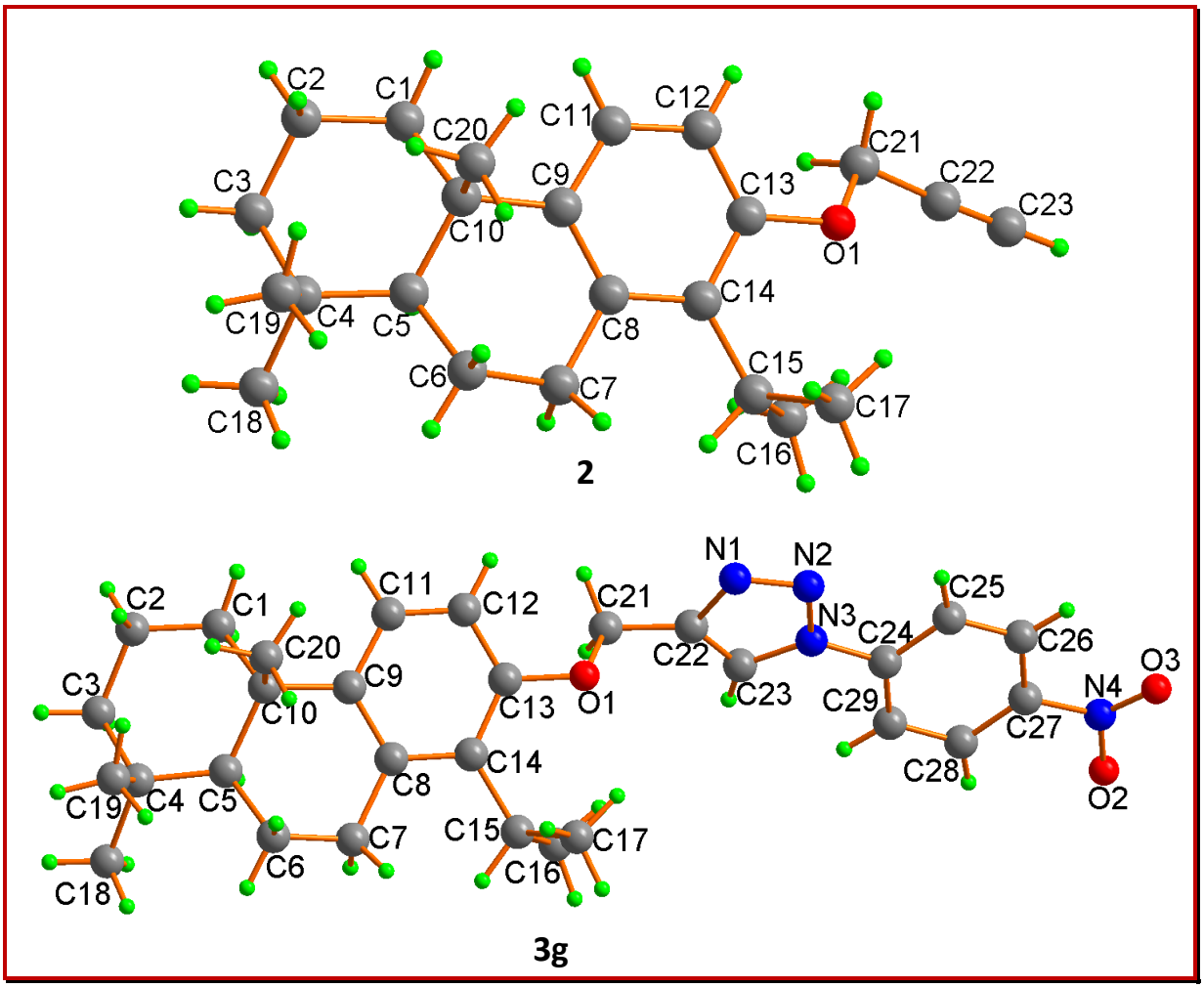

Figure 1: The structures of **2** and **3g** showing the atom numbering with ellipsoids drawn at the 50% probability level.

In crystal **2**, the central six-membered ring (C5- C10) assumes a screw boat conformation, as indicated by the total puckering amplitude QT = 0.533 (3) Å and spherical polar angle θ = 130.5 (3)° with φ = 104.2 (5)°, whereas the second insatured six-membered ring adopt a chair conformation with the following puckering parameters: QT = 0.543 (4) Å, θ =174.3 (4)°, φ= 335(4)°. The prop-2-yn-1-yloxy group (O1-C21-C22-C23) is twisted to the fused benzene ring with 35.8(3)°. As indicated in **Fig. 4**, the cohesion of the **2** structure is supported by C–H···H–C hydrogen bond interactions, C2–H2B···H23–C23 = 2.300(1) Å, between two neighbour molecules to form a helical arrangement chains along $\vec{b}$ axis**.** There are no other significant intermolecular interactions present.

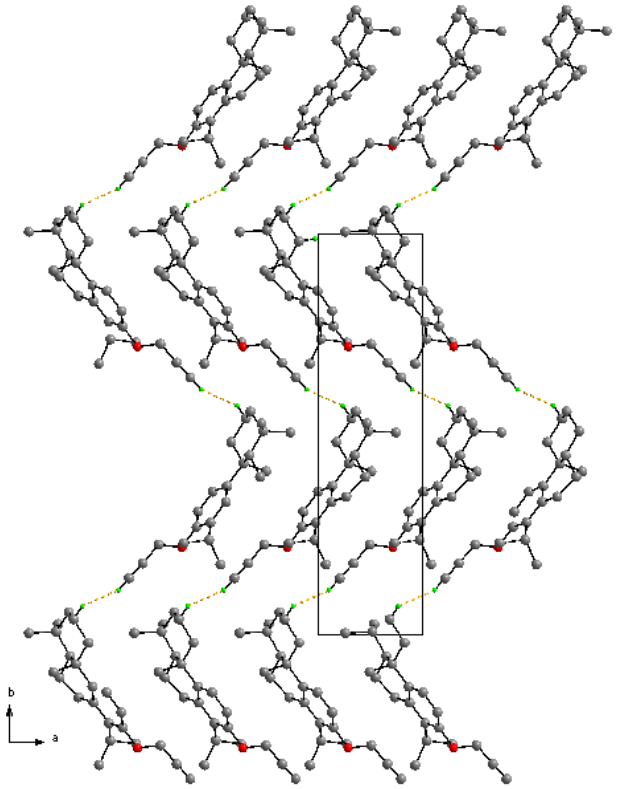

Figure 4: Crystal structure of **2** showing a chain viewed along the c-axis. For clarity, only the H atoms involved in the hydrogen bonds (dashed lines) interactions have been included.

In crystal structure **3g**, the central six-membered ring (C5-C10) assumes a half chair conformation, as indicated by the total puckering amplitude QT = 0.537 (6) Å and spherical polar angle θ = 48.6 (6)° with φ = 136.0 (8)°, whereas the second insatured six-membered ring exhibits a chair conformation [QT = 0.554 (4) Å, θ =176.9 (6)°, φ= 255(11)°]. The dihedral angle between the fused benzene ring and pyrazole and nitrophenyl plane are 54.9(3)° and 46.0(3)°, respectively. The angle between the nitophenyl and 1,2,3-triazole planes is 9.4(3)°. In the crystal, molecules are linked by C—H…O interactions, forming layers running along the (011) plane (**Table 3** and **Fig. 5**).

Similar conformation for the three fused rings has been reported previously with hydroxyl substituent, methyl acetate or benzoate in position C13 of both compounds [**23-25**].

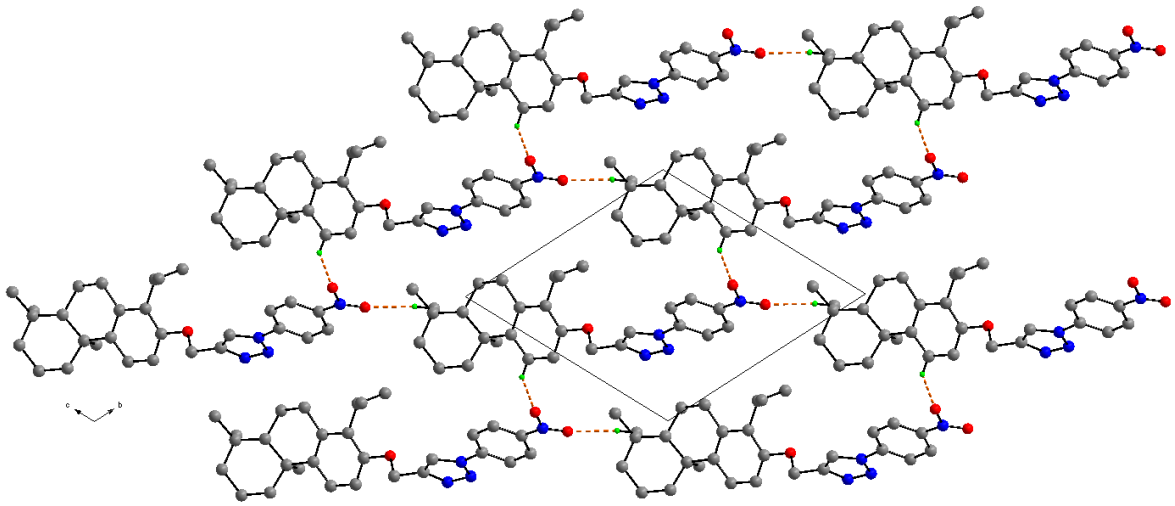

Figure 5: Crystal structure of **3g** in a view along the a-axis, showing C–H···O (dashed orange lines) hydrogen-interactions

Table 2: Selected experimental geometric parameters (Å, °) for compounds **2** and **3g**

		Compound 2	
Bond			
O1—C13	1.385(4)	C22—C23	1.160(6)
O1—C21	1.398(4)	C22—C21	1.441(6)
Angles			
C13—O1—C21	116.2(3)	C21—C22—C23	177.2(4)
O1—C21—C22	110.5(3)		
		Compound 3g	
O1—C13	1.331(5)	N1—N2	1.239(6)
O1—C6’	1.410(7)	N2—N3	1.406(6)
C22—C23	1.321(8)	N3—C21	1.350(6)
C22—C21	1.427(7)	N1—C22	1.435(7)
O2—N4	1.220(7)	N3—C23	1.357(7)
O3—N4	1.21(2)	N4—C24	1.380(7)
Angles			
C13—O1—C21	111.5(4)	O3—N4—O2	124.4(16)
N2—N1—C22	110.3(5)	O3—N4—C24	115.8(11)
N1—N2—N3	102.4(4)	O2—N4—C24	116.4(6)
C21—N3—C23	126.3(5)	O1—C21—C22	104.7(4)
C21—N3—N2	117.2(4)	N1—C22—C23	111.5(5)
C23—N3—N2	116.5(4)	N3—C23—C22	99.2(5)

Table 3

Hydrogen bonds (Å , °) for compound **3g**

D—H…A	**D—H**	**H…A**	**D…A**	**D—H…A**
C19 – H19C…O3^{i}	0.93	2.43	3.383(1)	136
C11– H11…O2^{ii}	0.96	2.61	3.345(12)	162

Symmetry codes: (i) -1 :-2+ x, -1 + y, 1-z; (ii) 2+x, 1+y, z

Hirshfeld analysis

Hirshfeld surface (HS) analysis plots generated using *CrystalExplorer17.5* shows the various intermolecular interactions in crystal structure (Fig. 6). The two-dimensional fingerprint plots are given in Fig. 7, showed the intermolecular contacts and their percentage distributions on the Hirschfeld surface. The red spots correspond to the H···H for **2** and O···H for **3g** (Fig. 6). In the view Hirshfeld surface mapped over the electrostatic potential in Fig. 6, the red and blue regions around the electronegative and electropositive atoms result from the polarization of charges about the acceptors and donors, respectively.

The Hirshfeld surface analysis for **2** is dominated by H…H contacts, representing van der Walls interactions (82.2%) with an evident sting at about $d_i = d_e = 1.1$ Å (Fig. 7b), corresponding to H2B…H23 ≈ 2.102 Å. The central green strip in Fig. 7b, centered at $d_e + d_i = 2.9$Å along the diagonal, indicates the presence of a large H…H contacts in the molecular packing. In the absence of C—H···π interactions, the pairs of characteristic wings in Fig. 7d arise from H···C/C···H contacts (14.6%) and are viewed as pairs of spikes with the tips at $d_e + d_i = 3.0$Å. All other contacts have a minor contribution to the crystal packing (H···O/O···H 1.5%, C···C 1.2% and O···C/C···O 0.4%).

The Hirshfeld surface analysis for **3g** shows the most important interaction is H···H contributing 55.7% to the overall crystal packing, which is reflected in Fig. 7b as widely scattered points at $d_i = d_e = 1.15$ Å, is due to the short interatomic H…H contacts. The contribution (17.4%) from the O···H/H···O contacts shows a pair of sharp spikes corresponding to the C—H···O interactions (Fig. 7c) and is viewed as pair of spikes with the tips at $d_e + d_i = 2.30$Å. The C···H/H···C and N···H/H···N interactions account for 13.6% and 10.8%, respectively (Fig. 7d and 7e), their interatomic distances are longer than the sum of their van der Waals radii. The small contributions from the remaining interatomic contacts : C···N/N···C (1.8%) and C···O/O···C (0.8%) have a negligible effect on the molecular packing.

The Hirshfeld surface analysis confirms the importance of H atoms contacts in estabilishing the packing. The large number of H...H and O...H/H...O interactions suggest that van der Waals interactions and hydrogen bonding play dominant role in stabilizing the lattice of the **2** and **3g** structures.

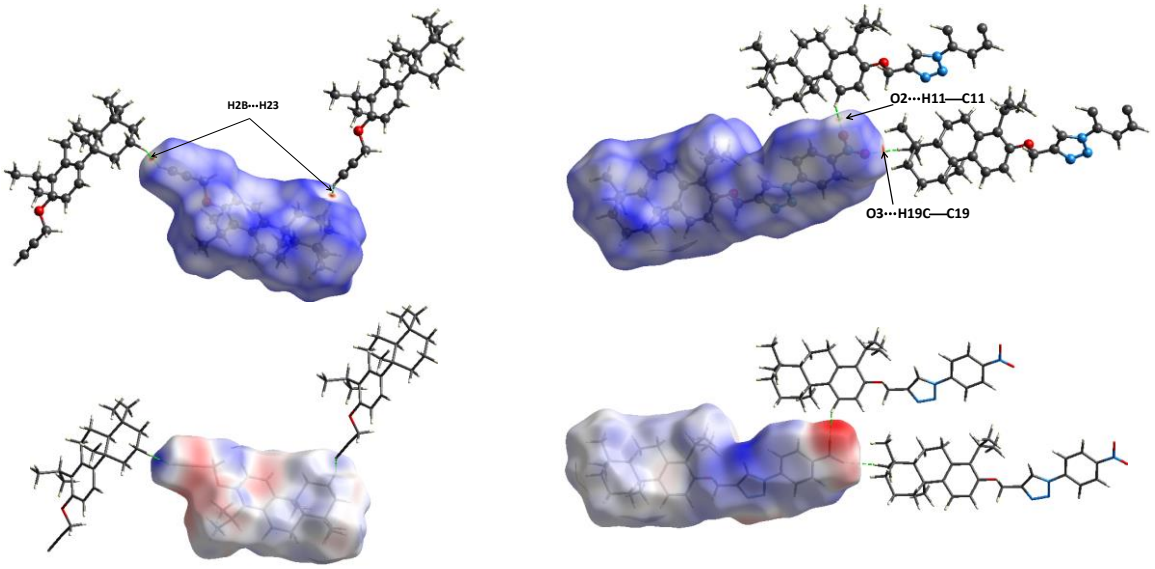

2 **3g**

Figure 6: View of the three-dimensional Hirshfeld surface of **2** and **3g** plotted over d_{norm} to visualize the intermolecular interactions.

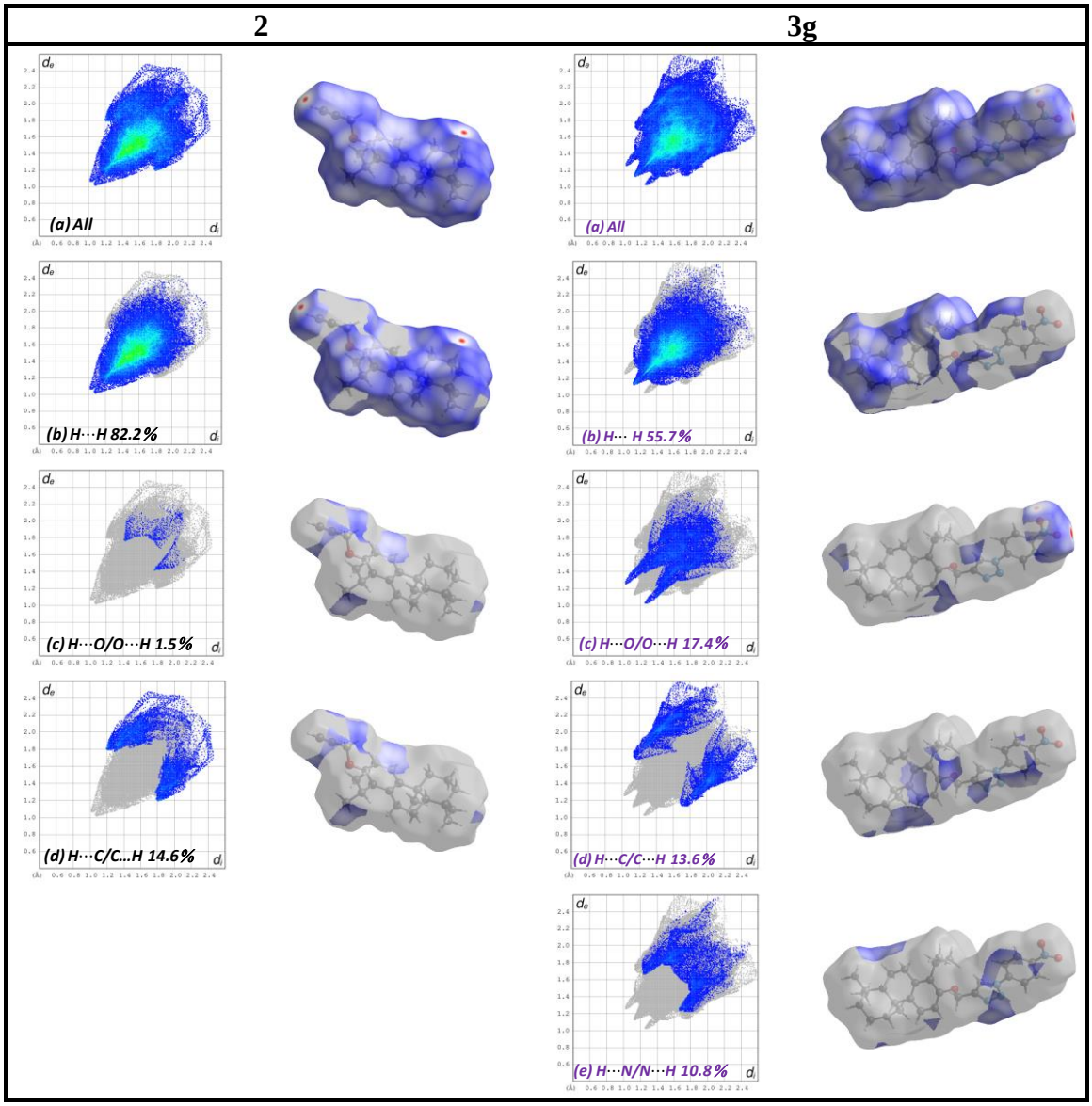

Figure 7: Relative contributions of intermolecular contacts to the Hirshfeld surface area in **2** and **3g** and 2D fingerprint plots of observed contacts

2.Anticancer activity

2.1.In vitro cytotoxic activity

Anti-Proliferative activity was carried out to examine the impacts of 1,2,3 triazole derivatives **3a-j** on the cell growth of four cancer cell lines, counting fibrosarcoma HT-1080, lung carcinoma A-549, and breast adenocarcinoma (MDA-MB-231 and MCF-7).The focused on cells were treated with diverse concentrations [**26**] of **3a-j** for 72h. The cytotoxic activity of the synthesized compounds was identified by MTT test, and IC_{50} values (concentration required to inhibit tumor cell proliferation by 50%) were recorded in Table 4, with Doxorubicin utilized as a positive control.

Table 4. Cytotoxic activity of **3a-j** against human HT-1080, A-549, MCF-7 and MDA-MB-231 cells for 72h.

Composé	IC_{50} (µM)			
	HT-1080	A-549	MCF-7	MDA-MB-231
3a	14.44	>50	31.37	>50
3b	19.25	18.62	32.02	25.33
3c	25.33	29.24	46.25	32.51
3d	21.08	26.02	23.10	19.09
3e	27.18	25.36	22.15	31.82
3f	> 50	42.02	28.22	> 50
3g	16.28	15.92	17.36	21.29
3h	24.51	20.58	31.97	27.16
3i	21.67	25.31	22.36	26.21
3j	19.74	24.23	25.90	24.32
Totarol	20.27	29.55	31.24	>50
Doxorubicin	1.03	0.97	0.51	1.22

From the screening results in Table 1, it was observed that compounds **3a-j** exhibited moderate to appreciable anticancer activity against the tested cancer cell lines. compound **3a** bearing a simple phenyl R moiety attached via triazole to the parent molecule totarol showed the most potent activity against HT-1080 cells line with IC_{50} of 14.44 µM. However compound **3f** containing an o-methyl-substituted phenyl group lost potency (IC_{50} > 50 and 42.02µM) against HT1080 and A549 cells compared with compound **3b** p-methylsubstituted group (IC_{50} = 19.25 and 18.62 µM, respectively). The activity profiles indicated that a methyl at the para-position on the phenyl group showed better activity than methyl at the ortho position. furthermore compound **3d** bearing a p-methoxyphenyl R moiety displayed appreciable anti-proliferative activity against MDA-MB-231 cells while as, it was moderately active towards the other three tested cell lines. Additionally, compounds **3c** and **3h** with p-chlorophenyl and m-chloro-o-methylphenyl R moieties respectively exhibited almost similar

activity as that of the totarol. In addition to this, compound **3g** bearing p-nitrophenyl R moiety, displayed impressive anti-proliferative activity with IC_{50} of 16.28, 15.92, 17.36 and 21.29 µM against HT-1080, A-549, MCF-7 and MDA-MB-231 cancer cell lines.These observations highlight the beneficial impact of substituents attached to phenyl R moiety towards the anti-proliferative activity. In addition compounds **3h, 3i** and **3j** with benzyl, phenacyl and ethylacetyl R moieties respectively exhibited almost similar activity as that of the totarol.

2.2.Annexin V binding

In further work, we selected compound **3g** among its derivatives synthesized for its antitumor activity (IC_{50}= 16.28µM) for further mechanistic investigations, and to verify specifically if the compound **3g** could induce apoptosis in HT-1080 and A549 cells. In terms of operating conditions, HT-1080 and A-549 human cancer cell lines were treated with compound **3g** at 15 µM concentration. After 24 h, the selected cells were stained with Muse TM Annexin V and Dead Cell kit, then counted using cytofluorimetric to detect the phosphatidyl serine membrane translocation (**Fig. 8**).

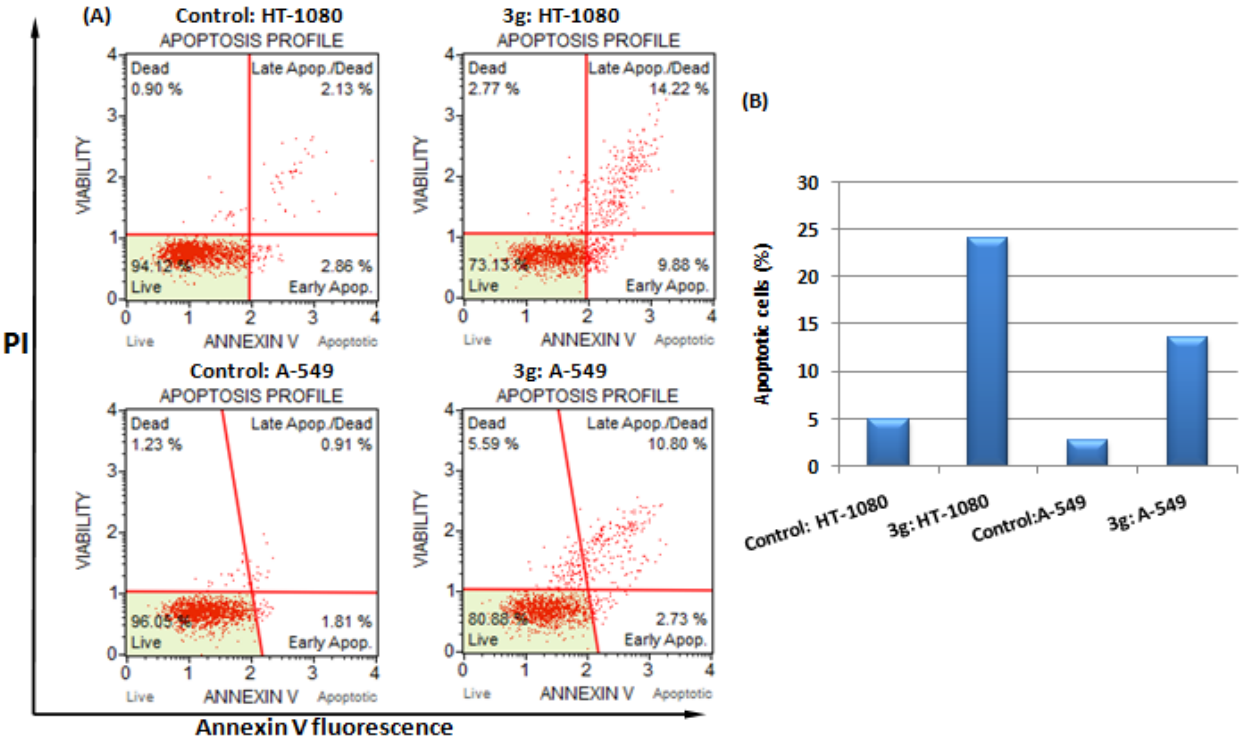

Fig. 8. Apoptosis effect on HT-1080 and A-549 cell line induced by compound **3g**. HT-1080 and A-549 cells were treated with compound **3g** with a unique concentration of 15 µM for 24 h, and apoptosis was measured by flow cytometry after staining with Annexin V/PI.

As shown in **Fig. 8.** Apoptotic cell death is generally moderate in both cells HT-1089 and A(549). In numerical terms, the percentage of HT-1080 total died cells (Early & Late apoptotic) increased to 24.1% after treatment with **3g** at the concentrations of 15 µM, in comparison with the cellules non traitées (4.99%) (Control). On the other hand, A-549 cells show a lower apoptotic death than HT-1080 cells, by a percentage increase of apoptotic cells that does not exceed 13.53%. This result demonstrated that the anti-proliferative activity observed when HT1080 cells were treated with **3g** could be the result of apoptosis.

2.3.Caspase-3 activity assay

In the suite, we investigated the activation of caspase-3 in compound **3g** treated cells, such as HT-1080 and A-549. Caspase-3 or executioner caspase is a family from a group of cysteine-aspartic acid proteases which play a key role in the apoptosis activation chain [**27**]. The same concentration (15 µM) of compound **3g**, HT-1080 and A-549 cells were treated and incubated for 24 h, then stained with Caspase 3/7 Kit. As shown in **Fig. 9**. the compound **3g** show a slight increase the percentage of caspase-3 activity cells (from 6.36% (ctrl) to 27.92% (15 µM), and (from 5.48% (ctrl) to 12.1% (15 µM) against the cells HT-1080 and A-549 respectively. Which indicated that compound **3g** induced apoptosis of HT-1080 and A-549 cancer cells in a independent manner.

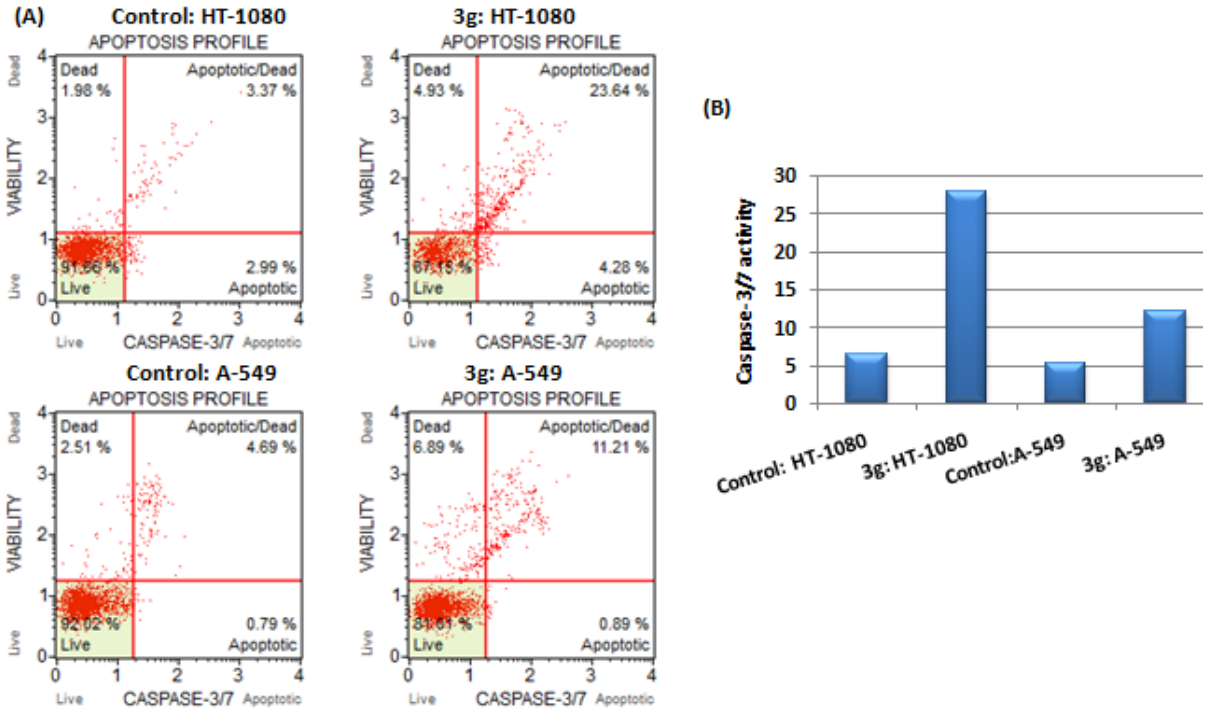

Fig. 9. The graph represents the enzymatic activity of caspase-3/7, during apoptotic event that occurs after the treatment of compound **3g** at 15 µM concentration in HT-1080 and A-549 cells for 24h. The values are means ±S.D of three independent experiments

2.4. Mitochondrial membrane potential(ΔΨm) depolarization

Also among the factual elements that are involved in cell death by the triggering of the apoptosis we find mitochondria membrane potential (MMP, ΔΨm) [**28**]. In this study, mitochondrial dysfunction was determined based on the MMP index that was measured by flow cytometry using the Muse MitoPotentialkit (Millipore-Merck). Selected cells (HT-1080 & A-549) were treated with **3g** at 15 µM unique concentration. results obtained after 24h as incubation time are grouped in **Fig. 10**.

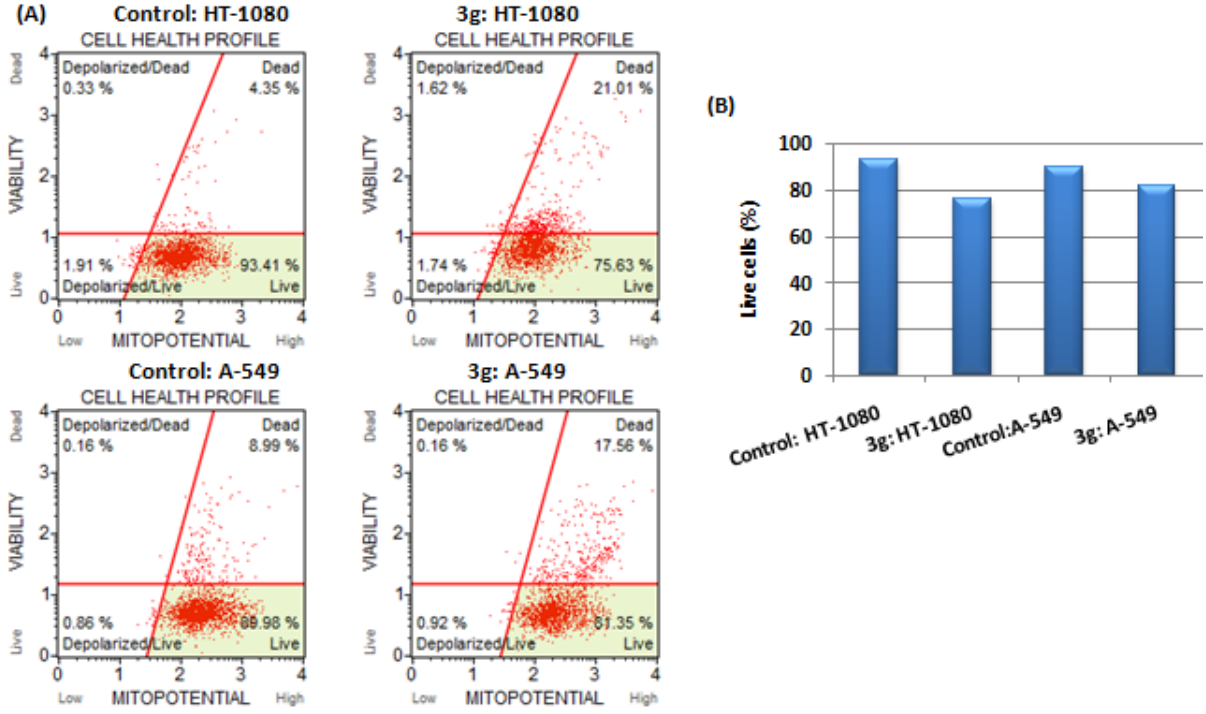

Fig. 10. Effect of the compound **3g** on the mitochondrial membranel potential (MMP) in HT-1080 and A-549 cells after treatment 15 µM concentrations during 24h.

As shown in **Fig. 10** the derivative **3g** did not induce a remarkable decrease in MMP index in both cases of cells. In statistical terms, a decrease in the percentage not exceeding 3% in the case of HT-1080 cells and 6% in the case of A-549 cells by contribution to their control. This suggests that the triazolyl analogs of totarol derivative **3g** is able to induce cell death independently of the mitochondrial pathway.

2.5. Investigation of cell cycle distribution

As an extension of our extensive study, the same compound **3g** was chosen to analyze the effect on cell cycle progression and induction of apoptosis in the HT-1080 and A-549 cell lines. HT-1080 and A-549 cells were treated with **3g** at 15 µM for 24 h. the results obtained

after the analysis of the effect on the normal cells (without anticancer agent) cycle profile and induction of apoptosis (with anticancer agent)have been shown in **Fig. 11.**

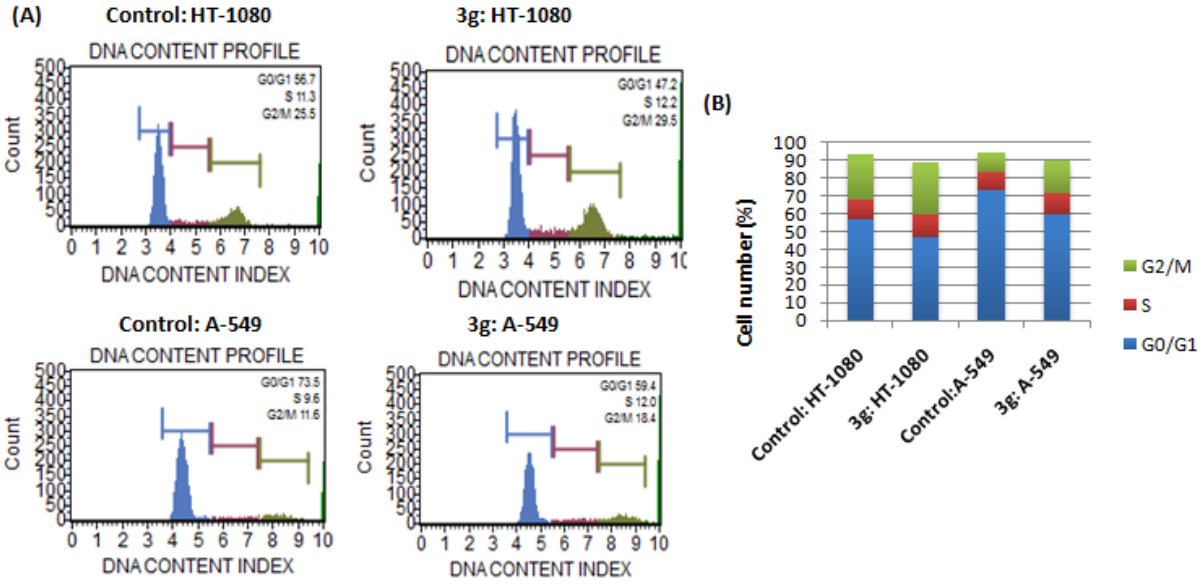

Fig. 11. Effect of compound **3g** on cell cycle was determined by PI staining using flow cytometric analysis

For cell line HT-1080 and in comparison with its reference, triazolyl analogs of totarol **3g** induced an average increase in the percentage of cells at G2/M and noteable decrease in G0/G1 from 56% to 47%. also, A-549 cells have been shown an average accumulation of cells in G2/M phase, a decrease in the pace that represents the G0/G1 phase from 73% to 59%. From the experimental results, cell cycle arrest of HT-1080 and A-549 cell lines in the G2/M phase may be due to degradation or fragmentation of the genetic materials confirming a role of apoptosis in compound **3g** induced cancer cell death.

Conclusion

The current study is the first report involving the synthesis of triazolyl analogs of totarol. In this study, we have synthesized a diverse of novel triazolyl analogs of totarol prepared through Cu(I) catalyzed click chemistry approach and characterized by the analysis spectral screened for anticancer activity against four human cancer cell lines. all Compounds showed weak activities against the tested four cancer cell lines, especially compound **3g,** it was more potent than totarol against all tested human cancer cell lines. The results of apoptosis assay and cell cycle analysis demonstrated that **3g** could obviously inhibit the proliferation of HT-1080 and A-549 cancer cells by inducing apoptosis in an independent caspase3/7 and arresting the cell cycle at G2/M phase.

Experimental section

All chemicals were used as obtained from commercial sources (Aldrich and Acros). Melting points (m.p.) were determined using a Kofler bench appa-ratus and are uncorrected.Analytical thin-layer chromatography (TLC) was performed on plates precoated with E. Merck silica gel 60 F254 to a thickness of 0.25 mm.IR spectra were recorded on a Bruker Vertex 70 spectro-photometer using potassium bromide discs in the frequency range 4000–400 cm–1 . HRMS were obtained on a Q-TOF micromass spectrometer. 1H and 13C NMR spectra were recorded on a Bruker Avance 300 (75) MHz spectrometer. Chemical shifts (δ) are expressed in parts per million (ppm) and coupling constants (*J*) are mentioned in Hz. They were recorded relative to the solvent $CDCl_3$ signal (7.26 and 77.16 ppm).

General procedure for the extraction of Totarol 1 from *Tetraclinis articulata* [**28**]

Powdered wood of Tetraclinis articulata (500 g) was exhaustively extracted by maceration with dichloromethane at room temperature for 24 h under agitation. The solvent was removed in a rotavapor and the residue obtained (26 g) was chromatographed in a silica gel column eluting with a solvent gradient hexane– EtOAc (9:1 v/v) affording 2.1 g of Totarol , whose identification was confirmed on the basis of its spectroscopic analyses.

General procedure for O-propargylation of totarol 2

To a round bottom flask containing K_2CO_3 (1.5 eq) and anhydrous acetone (100 mL), Totarol (2 eq) was added. The resulting mixture was vigorously stirred and after 30 min propargyl bromide solution (80% in toluene) was added to the reaction mixture that was kept under stirring at room temperature for 24 h. Afterwards, the mixture was extracted with ethyl acetate The crude reaction product was purified by silica gel column chromatography eluted with a mixture of hexane/ ethyl acetate (98:2), affording compound **2**.

General procedure for synthesis of azides

The azides were prepared as per the known method [**26**]. An aromatic amine (1 mmol) was ground in a mortar with silica sulfuric acid (0.70 g), for 1 min. Then $NaNO_2$ (2.5 mmol, 0.175 g), was added and the mixture was ground for 5–10 min to give the corresponding aryl diazonium silica sulfate. Then, NaN_3 (2.5 mmol, 0.163 g) in H_2O(4 mL) was added gradually and the reaction mixture was stirred at rt for 20 min. The mixture was diluted with EtOAc (10 mL) and was filtered after vigorous stirring. The residue was extracted with EtOAc (3 x12

mL) and the combined organic layer was washed with 5% NaOH solution (12 mL) and then dried over anhydrous Na_2SO_4. The solvent was evaporated to afford aromatic azides.

Compound 2

Yield: 80%; White solid, m.p.: 84–86 °C; IR (KBr, cm^{-1}): 3311, 3076 (C-H), 2930, 2132 (C≡C), 1634, 1587 (C=C), 1205, 1046(C-O).; ^{1}H NMR ($CDCl_3$) δ 7.24 (1H, d, J = 8.8, H-11), 6.74 (1H, d, J = 8.8, H-12), 4.78 (2H, d, J = 2.4 ,OCH2), 3.41 (1H, m, H-15), 3.09 (1H, dd, J = 17, 6.3, H-7β), 2.95 (1H, m, H-7α), 2.58 (1H, t, J = 2.4 Hz, H-23), 2.40 (1H, br d, J = 11.6, H-1β), 2.12-1.51 (8H, m), 1.36 (6H, 2 ×d like t with J = 7 Hz, H-16, H-17),1.34 (3H, s, H-20), 1.10 (3H,s, H-18), 1.06 (3H,s, H-19).^{13}C NMR (75 MHz, CDCl3): δ 154.4, 143.8, 133.8, 127.9, 122.7, 110.6, 74.8, 55.5, 50.5, 49.8, 41.9, 39.9 , 38.0 , 33.6, 33.5 , 29.1, 27.8, 25.5, 21.9, 20.9, 19.8, 19.7; HRMS: m/z $[M+H]^+$ Calcd. for $C_{23}H_{33}O$: 325.2526 found: 325.2735.

General Procedure for the Synthesis of Triazoles

The alkynyl totarol (1 eq) and the corresponding azide (1 eq) were dissolved in EtOH/H_2O (1:1), followed by the addition of $CuSO_4 \cdot 5H_2O$ (20 mol %) and sodium ascorbate (40 mol %). The mixture was stirred at room temperature for 24 h. The reaction was stopped by adding H_2O, extracted with CH_2Cl_2, dried over anhydrous Na_2SO_4, concentrated and purified by column chromatography on silica gel.

Compound 3a

Yield 70%; Yellow solid; mp 168–170 °C; IR (KBr, cm^{-1}): 3159, 3048 (C-H, triazole), 2956,2895 (C-H), 1678 (C=N), 1551,1467 (C=C), 1212, 1078 (C-O).^{1}H NMR ($CDCl_3$) δ 8.04 (1H, s, 1H-riazole), 7.77 (2H, d, *J* = 7.5 Hz, H-Ar), 7.51 (3H, m, H-Ar), 7.14 (1H, d, *J* = 8.8 Hz, H-11), 6.90 (1H, d, *J* = 8.8 Hz, H-12), 5.19 (2H, s, OCH_2), 3.45 – 3.24 (1H, m, H-15), 2.99 (1H, dd, *J* = 16.9, 6.6 Hz, H-7β), 2.80 (1H, ddd, *J* = 16.9, 11.3, 6.6 Hz, H-7α), 2.35 – 2.21 (1H, m), 2.01 – 1.43 (6H, m), 1.38 (6H, 2*d like t with *J* = 7.0 Hz, H-16, H-17), 1.20 (3H, s, H-20), 0.97 (3H, s, H-18), 0.95 (3H, s, H-19). ^{13}C NMR (75 MHz, $CDCl_3$) δ 154.8, 146.0, 143.9, 137.1, 134.0, 133.5, 129.8, 128.8, 123.0, 120.6, 120.6, 110.5, 62.2, 49.5, 41.6, 39.6, 37.8, 33.3, 33.3, 28.8, 27.5, 25.2, 21.6, 20.7, 19.5, 19.4. HRMS: m/z $[M+H]^+$ Calcd. for $C_{29}H_{38}N_3O$: 444.3009 found: 444.3026.

Compound 3b

Yield 73%; White solid; mp 194–196 °C; IR (KBr, cm^{-1}): 3133 (C-H, triazole), 2924, 2869 (C-H), 1587 (C=N), 1518, 1475 (C=C), 1258, 1045, (C-O).;^{1}H NMR ($CDCl_3$) δ 7.98 (1H,s,H-triazole), 7.61 (2H,d, *J* = 8.3 Hz, H-Ar), 7.32 (2H, d, *J* = 8.3 Hz, H-Ar), 7.12 (1H, d, *J* = 8.8 Hz, H-11), 6.88 (1H, d, *J* = 8.8 Hz, H-12), 5.27 (2H, s, OCH_2), 3.40 – 3.18 (1H, m, H-15), 2.96 (1H, dd, *J* = 17.6, 6.5 Hz, H-7β), 2.77 (1H, ddd, *J* = 17.6, 11.3, 6.5 Hz, 1H-7α), 2.42 (3H, s, CH_3), 2.26 (1H, br d, *J* = 12.7 Hz, H-1β), 2.01 – 1.38 (5H, m), 1.37 – 1.29 (6H, 2*d like t, *J* = 7.0 Hz, H-16, H-17), 1.19 (3H, s, H-20), 0.95 (3H, s, H-18), 0.91 (3H, s, H-19).^{13}C NMR (75 MHz, $CDCl_3$) δ 154.9, 145.9, 143.9, 139.0, 134.9, 134.0, 133.5, 130.3, 123.0, 120.6, 110.5, 62.3, 49.6, 41.6, 39.7, 37.8, 33.3, 33.4, 28.9, 27.6, 25.3, 21.7, 21.2, 20.7, 19.5, 19.5. HRMS: m/z $[M+H]^+$ Calcd. for $C_{30}H_{40}N_3O$: 458.3166 found: 458.3179.

Compound 3c

Yield 75 %; white solid; mp 223-235 °C; IR (KBr, cm^{-1}): 3148 (C-H, triazole), 2922, 2885 (C-H), 1638 (C=N), 1591, 1492 (C=C), 1258, 1007, (C-O), 1095 (C-Cl).;^{1}H NMR (300 MHz, $CDCl_3$) δ 7.99 (1H, s, H-triazole), 7.69 (2H, d, *J* = 8.9 Hz, H-Ar), 7.50 (2H, d, *J* = 8.9

Hz, H-Ar), 7.10 (1H, d, *J* = 8.8 Hz, H-11), 6.85 (1H, d, *J* = 8.8 Hz, H-12), 5.28 (2H, s, OCH_2), 3.29 (1H, m, H-15), 2.97 (1H, dd, *J* = 17.1, 6.5 Hz, H-7β), 2.77 (1H, ddd, *J* = 17.1, 11.2, 6.5 Hz, H-7α), 2.30 – 1.43 (m, 7H), 1.33 (2*d like t, *J* = 7.0 Hz, 6H), 1.19 (3H, s, H-20), 0.96 (3H, s, H-18), 0.91 (3H, s, H-19). ^{13}C NMR (75 MHz, CDCl3) δ 154.9, 146.4, 144.1, 135.8, 135.8, 134.8, 133.7, 130.1, 123.1, 121.9, 120.5, 110.7, 77.5, 62.4, 49.7, 41.8, 39.8, 37.9, 33.4, 33., 29.8, 28.9, 27.7, 25.3, 21.7, 20.8, 19.6, 19.5. HRMS: m/z $[M+H]^+$ Calcd. for $C_{29}H_{40}ClN_3O$: 478.2620 found: 478.2635.

Compound 3d

Yield 70%; Yellow oil; IR (KBr, cm^{-1}): 3091 (C-H, triazole), 2928,2876 (C-H), 1608 (C=N), 1501, 1462 (C=C), 1253, 1039, (C-O).; ^{1}H NMR ($CDCl_3$) δ 7.92 (s, H-triazole), 7.64 (2H, d, *J* = 9.0 Hz, H-Ar), 7.11 (1H, d, *J* = 8.8 Hz, H-11), 7.01 (2H, d, *J* = 9.0 Hz, H-Ar), 6.86 (1H, d, *J* = 8.8 Hz, H-12), 5.22 (2H, s, OCH_2), 3.81 (3H, s, OCH_3), 3.42 – 3.19 (1H, m, H-15), 2.98 (1H, dd, *J* = 17.1, 6.5 Hz, H-7β), 2.74 (1H, m, H-7α), 2.26 (1H, d, *J* = 12.4 Hz, H-1β), 2.18 – 1.38 (m, 6H), 1.33 (6H, 2*d like t, *J* = 7.0 Hz, H-16, H-17), 1.19 (3H, s, H-20), 0.94 (3H, s, H-18), 0.91 (3H, s, H-19).^{13}C NMR (75 MHz, $CDCl_3$) δ 150.9, 145.6, 143.4, 139.0, 134.9, 134.0, 133.5, 130.3, 123.0, 120.6, 111.5, 62.3, 49.5, 41.6, 39.6, 37.8, 34.3, 33.3, 28.9, 27.6, 25.3, 21.7, 21.22, 20.6, 19.5, 19.4.; HRMS: m/z $[M+H]^+$ Calcd. for $C_{30}H_{40}N_3O_2$: 473.3115 found: 473.3136.

Compound 3e

Yield 84%; Red solid; mp 134–136 °C; IR (KBr, cm^{-1}): 3157, 3071 (C-H, triazole), 2957, 2876 (C-H), 1578 (C=N), 1509, 1456 (C=C), 1211, 1045,(C-O);.^{1}H NMR (300 MHz, $CDCl_3$) δ 7.77 (1H, s, H triazole), 7.50 (1H, dd, *J* = 6.3, 3.0 Hz, H-Ar), 7.24 (2H, d, *J* = 3.0 Hz, H-Ar),7.10 (d, *J* = 8.8 Hz, H-11), 6.85 (1H, d, *J* = 8.8 Hz, H-12), 5.26 (2H, s, OCH_2), 3.37 – 3.18 (1H, m, H-15), 2.97 (1H, dd, *J* = 17.1, 6.5 Hz, H-7β), 2.73 (1H, ddd, *J* = 17.1, 11.3, 6.5 Hz, H-7α), 2.17 (3H, s, CH_3), 2.14 – 1.35 (6H, m), 1.29 (6H, 2*d like t *J* = 7.0 Hz, H-16, H-17), 1.17 (3H, s, H-20), 0.93 (3H, s, H-18), 0.89 (3H, s, H-19).^{13}C NMR (75 MHz, $CDCl_3$) δ 154.8, 145.3, 143.8, 137.6, 136.0, 133.9, 133.5, 132.8, 130.8, 127.2, 124.9, 124.2, 122.9, 110.5, 62.2, 49.5, 41.6, 39.6, 37.7, 33.3, 33.2, 28.8, 27.5, 25.2, 21.6, 20.6, 19.5, 19.4. HRMS: m/z $[M+H]^+$ Calcd. for $C_{30}H_{39}ClN_3O$: 492.2776 found: 492.2787.

Compound 3f

Yield 80%; Yellow solid; mp 150–152 °C; IR (KBr, cm^{-1}): 3109, 3045 (C-H, triazole), 2987 ,2895 (C-H), 1508 (C=N), 1547, 1502 (C=C), 1238, 1167,1075, (C-O).; ^{1}H NMR ($CDCl_3$) δ 7.84 (1H, s, H-triazole), 7.40 (4H, m, H-Ar), 7.16 (1H, d, *J* = 8.8 Hz,H-11), 6.92 (1H, d, *J* = 8.8 Hz,H-12), 5.36 (1H, s, OCH_2), 3.45 – 3.22 (1H, m, H-15), 3.00 (1H, dd, *J* = 17.2, 6.6 Hz, H-7β), 2.81 (1H, ddd, *J* = 17.2, 11.3, 6.6 Hz, H-7α), 2.25 (3H, s, CH_3), 2.02 – 1.43 (6H, m), 1.41 – 1.32 (6H, 2*d like t with J= 6.9 Hz, H-16,H-17), 1.24 (3H, s, H-20), 0.99 (3H, s, H-18), 0.96 (3H, s, H-19).^{13}C NMR (75 MHz, $CDCl_3$) δ 154.8, 145.0, 143.8, 136.5, 133.9, 133.6, 133.4, 131.5, 129.9, 126.9, 126.0, 124.0, 122.9, 110.4, 62.3, 49.5, 41.6, 39.6, 37.7, 33.3, 33.2, 28.8, 27.5, 25.2, 24.0, 21.6, 20.6, 19.5, 19.4, 17.8. HRMS: m/z $[M+H]^+$ Calcd. for $C_{30}H_{39}N_3O$: 458.3166 found: 458.3182.

Compound 3g

Yield 70%; Yellow Crystal,; mp 236–238 °C; IR (KBr, cm^{-1}): 3145 (C-H, triazole), 2915, 2864 (C-H), 1599 (C=N), 1526, 1473 (C=C), 1295, 1008 (C-O).; ^{1}H NMR ($CDCl_3$) δ 8.43 (1H, d, J = 9.0 Hz, H-2"), 8.17 (1H, s, H-triazole), 8.02 (1H, d, J = 9.0 Hz, H-3"), 7.14 (1H, d, J = 8.8 Hz, H-11), 6.87 (1H, d, J = 8.8 Hz, H-12), 5.31 (1H, s, OCH_2), 3.34 (1H, m, H-15), 2.99 (1H, dd, J = 17.2, 6.6 Hz, H-7β), 2.79 (1H, ddd, J = 17.2, 11.3, 6.6 Hz, H-7α), 2.33 – 2.20 (d, J = 13.2 Hz, H-1β), 2.02 – 1.86 (1H, m), 1.85 – 1.40 (6H, m), 1.35 (6H, 2*d like t, J =

6.8 Hz, H-16,H-17), 1.20 (3H, s, H-20), 0.97 (3H, s, H-18), 0.93 (3H, s, H-19). ^{13}C NMR (75 MHz, CDC_{l3}) δ 154.7, 147.3, 147.0, 144.1, 141.2, 134.1, 133.6, 125.6, 123.0, 120.6, 120.4, 110.4, 62.1, 49.5, 41.6, 39.7, 37.8, 33.3, 28.8, 27.5, 25.2, 21.6, 20.7, 19.5, 19.4. ; HRMS: m/z $[M+H]^+$ Calcd. for $C_{29}H_{36}N_4O_3$: 489.2860 found: 489.2896.

Compound 3h

Yield 80%; Yellow solid; mp 150-152 °C; IR (KBr, cm^{-1}): 3136 (C-H, triazole), 2963 (C-H), , 1754 (C=O), 1625 (C=N), 1509, 1458, (C=C),, 1210, 1036 (C-O). ^{1}H NMR (300 MHz, $CDCl_3$) δ 7.79 (1H, s, H-triazole), 7.11 (1H, d, *J* = 8.7 Hz, H-11), 6.85 (1H, d, *J* = 8.7 Hz, H-12), 5.26 (2H, s, OCH_2), 5.19 (2H, s, CH_2CO), 4.28 (3H, q, *J* = 7.0 Hz, CH_2-CH_3), 3.43 – 3.22 (1H, m, H-15), 2.99 (1H, dd, *J* = 17.1, 6.6 Hz, H-7β), 2.80 (1H, ddd, *J* = 17.1, 11.2, 6.6 Hz, H-7α), 2.30 (1H, d, *J* = 12.4 Hz, 1H-1β), 2.07 – 1.40 (7H,m), 1.37 – 1.25 (6H, 2*d like t, *J* = 7.4 Hz, H-16, H-17), 1.22 (3H, s, H-20), 0.99 (3H, s, H-18), 0.94 (3H, s, H-19).^{13}C NMR (75 MHz, $CDCl_3$) δ 166.2, 154.8, 145.4, 143.6, 133.8, 133.4, 123.8, 122.8, 110.3, 62.3, 62.1, 50.9, 49.5, 41.5, 39.6, 37.7, 33.2, 33.2, 28.7, 27.4, 25.1, 21.5, 20.5, 19.4, 19.3, 14.0. HRMS: m/z $[M+H]^+$ Calcd. for $C_{27}H_{40}N_3O_3$: 454.3064 found: 454.3083.

Compound 3i

Yield 72%; White solid; mp 174–176 °C; IR (KBr, cm^{-1}): 3131, 3088 (C-H, triazole), 2924, 2860 (C-H), 1625 (C=N), 1588, 1468 (C=C), 1258, 1041 (C-O).; ^{1}H NMR ($CDCl_3$) δ 7.48 (1H, s, H-triazole), 7.34 (2H, m, H-Ar), 7.22 (3H, m, H-Ar), 7.05 (1H, d, *J* = 8.8 Hz, H-11), 6.77 (1H, d, *J* = 8.8 Hz, H-12), 5.51 (2H, s, OCH_2), 5.14 (2H, s, CH_2Ph), 3.33 – 3.12 (1H, m, H-15), 2.91 (1H, dd, *J* = 17.1, 6.6 Hz, H-7β), 2.71(1H, ddd, *J* = 17.1, 11.3, 6.6 Hz, H-7α), 2.21 (1H, d, *J* = 12.7 Hz, H-1β), 2.05 – 1.28 (5H, m), 1.25 – 1.18 (6H, 2*d like t , *J* = 6.0 Hz, H-16, H-17), 1.15 (3H, s, H-20), 0.91 (3H, s, H-18), 0.89 (3H, s, H-19).^{13}C NMR (75 MHz, $CDCl_3$) δ 155.0, 145.7, 143.8, 134.9, 133.9, 133.6, 129.2, 128.8, 128.0, 122.9, 122.4, 110.7, 62.5, 54.2, 49.7, 41.7, 39.7, 37.8, 33.4, 33.3, 29.8, 28.8, 27.5, 25.2, 21.7, 20.6, 19.6, 19.5. HRMS: m/z $[M+H]^+$ Calcd. for $C_{30}H_{40}N_3O$: 458.3166 found: 458.3183.

Compound 3j

Yield 74%; Yellow solid; mp 198–200 °C; IR (KBr, cm^{-1}): 3079, 3048 (C-H, triazole), 2994 (C-H), , 1778 (C=O), 1561 (C=N), 1522 (C=C),1110, 1077(C-O) .; ^{1}H NMR ($CDCl_3$) δ 8.00 (2H, m, H-Ar), 7.80 (s, H-triazole), 7.70 – 7.43 (3H, m, H-Ar), 7.12 (1H, d, *J* = 8.8 Hz, H-11), 6.86 (1H, d, *J* = 8.8 Hz, H-12), 5.88 (2H, s, CH_2CO), 5.25 (2H, s, OCH_2), 3.29 (1H, m, H-15), 2.97 (1H, dd, *J* = 17.1, 6.5 Hz, H-7β), 2.75 (1H, ddd, *J* = 17.6, 11.4, 7.8 Hz, H-7α), 2.34 – 1.36 (6H, m), 1.32 (6H, 2*d like t with *J* = 7.0 Hz, H-16, H-17), 1.20 (3H, s, H-20), 0.98 (3H, s, H-18), 0.93 (3H, s, H-19).^{13}C NMR (75 MHz, $CDCl_3$) δ 190.3, 154.9, 145.4, 143.7, 134.6, 133.9, 133.5, 133.3, 129.1, 128.1, 124.4, 122.9, 110.4, 62.2, 55.5, 49.5, 41.6, 39.6, 37.7, 33.3, 33.2, 28.8, 27.5, 25.2, 21.6, 20.6, 19.5, 19.4. HRMS: m/z $[M+H]^+$ Calcd. for $C_{31}H_{40}N_3O_2$: 486.3115 found: 486.3138.

Structure solution and refinement

The X-Ray diffraction studies of crystals 2 and 3g Intensity data were performed on a Bruker DUO APEX 2 CCD diffractometer using graphite-monochromated Mo-Kα radiation (*λ*= 0.71073 Å) at room temperature (298K). More than a hemisphere of three-dimensional XRD data was collected with frame widths of 0.5° in ω, and a 30 s count time for each frame. The data was corrected for absorption using a multi-scan type model in the program SADABS

[**29**]. The structure were determined by the direct method and was refined by full matrix least squares based on F^2 using SHELXL program implanted in the WINGX program package [**30-31**]. The molecular graphic were drawn using the *DIAMOND* programs [**32**]. Details on the crystallographic studies, as well as atomic displacement parameters, are given as Supporting Information in the form of cif files. The non-hydrogen atoms were refined with anisotropic thermal parameters. H-atoms were positioned geometrically and refined using a riding model with C–H = 0.93 – 0.98 Å, and with U_{iso}(H) = 1.2 U_{eq}(C) or 1.5 U_{eq}(C-methyl). All non-hydrogen atoms were refined anisotropically. For **3g**, difference Fourier calculation indicated disorder in the O3 nitro group and was refined with two positions (0.52(1)/0.48(1)).

Hirshfeld surface analysis

The Hirshfeld surfaces calculated for **2** and **3g** structures were analysed to clarify the nature of the intermolecular interactions between different units in the crystal packing motifs. Thus, a Hirshfeld surface analysis [**33**] and the associated two-dimensional fingerprint plots [**34**] were performed using CrystalExplorer17.5 [**35**]. The 3D d_{norm} surfaces are mapped over a fixed colour scale of -0.0718 to 1.3075 for **2**, and -0.2191 to 1.3685 a.u. for **3g**. The electrostatic potential were generated using *TONTO* implanted in Crystal Explorer 17.5 with the STO-3G basis set at the Hartree–Fock level of theory, energy in the range -0.0368 to +0.0520 a.u for **2** and -0.0836 to +0.0617 a.u for **3g**.

References

[1] S. Antoni, J. Ferlay, I. Soerjomataram, A. Znaor, A. Jemal, and F. Bray, "Bladder Cancer Incidence and Mortality: A Global Overview and Recent Trends," European Urology, vol. 71, no. 1. Elsevier B.V., pp. 96–108, Jan. 01, 2017, doi: 10.1016/j.eururo.2016.06.010.

[2] Z. Xu et al., "Design, Synthesis, and Evaluation of Tetraethylene Glycol-Tethered Isatin–1,2,3-Triazole–Coumarin Hybrids as Novel Anticancer Agents," Journal of Heterocyclic Chemistry, vol. 56, no. 3. pp. 1127–1132, 2019, doi: 10.1002/jhet.3475.

[3] J. Zugazagoitia, C. Guedes, S. Ponce, I. Ferrer, S. Molina-Pinelo, and L. Paz-Ares, “Current Challenges in Cancer Treatment,” Clinical Therapeutics, vol. 38, no. 7. Excerpta Medica Inc., pp. 1551–1566, Jul. 01, 2016, doi: 10.1016/j.clinthera.2016.03.026.

[4] G. M. Cragg and J. M. Pezzuto, “Natural Products as a Vital Source for the Discovery of Cancer Chemotherapeutic and Chemopreventive Agents,” Med. Princ. Pract., vol. 25, no. 2, pp. 41–59, 2016, doi: 10.1159/000443404.

[5] S. Dutta, S. Mahalanobish, S. Saha, S. Ghosh, and P. C. Sil, “Natural products: An upcoming therapeutic approach to cancer,” Food Chem. Toxicol., vol. 128, no. April, pp. 240–255, 2019, doi: 10.1016/j.fct.2019.04.012.

[6] and K. I. Haragushi H, Ishikawa H, “Antioxidant action of diterpenoids from Prodocarpas nagi.,” Planta Medica., vol. 63, no. 5, pp. 213–215, 1997.

[7] C. Tacon, E. M. Guantai, P. J. Smith, and K. Chibale, “Synthesis, biological evaluation and mechanistic studies of totarol amino alcohol derivatives as potential antimalarial agents,” Bioorganic Med. Chem., vol. 20, no. 2, pp. 893–902, 2012, doi: 10.1016/j.bmc.2011.11.060.

[8] W. E. Campbell, “In Vitro Antiplasmodial Activity of Abietane and Totarane Diterpenes Isolated from Harpagophytum procumbens (Devil ’ s Claw),” pp. 720–724, 2003.

[9] K. Yamaji, S. Mori, M. Akiyama, A. Kato, and T. Nakashima, “The antifungal compound totarol of Thujopsis dolabrata var. hondai seeds selects for fungi on seedling root surfaces,” J. Chem. Ecol., vol. 33, no. 12, pp. 2254–2265, Dec. 2007, doi: 10.1007/s10886-007-9390-2.

[10] T. Xu et al., “Totarol, a natural diterpenoid, induces selective antitumor activity in SGC-7901 human gastric carcinoma cells by triggering apoptosis, cell cycle disruption and suppression of cancer cell migration,” J. B.U.ON., vol. 24, no. 2, pp. 686–692, 2019.

[11] S. Mahdjour et al., “Synthesis and antiproliferative activity of podocarpane and totarane derivatives,” Eur. J. Med. Chem., vol. 158, pp. 863–873, 2018, doi: 10.1016/j.ejmech.2018.09.051.

[12] Y. Jia, C. Wu, B. Zhang, Y. Zhang, and J. Li, “Ferruginol induced apoptosis on SK-Mel-28 human malignant melanoma cells mediated through P-p38 and NF-κB,” Hum. Exp. Toxicol., vol. 38, no. 2, pp. 227–238, 2019, doi: 10.1177/0960327118792050.

[13] B. Zhang, “Comprehensive review on the anti-bacterial activity of 1,2,3-triazole hybrids,” European Journal of Medicinal Chemistry, vol. 168. Elsevier Masson SAS, pp. 357–372, Apr. 15, 2019, doi: 10.1016/j.ejmech.2019.02.055.

[14] M. H. Shaikh et al., “,2,3-Triazole Derivatives as Antitubercular Agents: Synthesis, Biological Evaluation and Molecular Docking Study 1,2,3-Triazole Derivatives as Antitubercular Agents: Synthesis, Biological Evaluation and Molecular Docking Study.” Accessed: Jun. 02, 2020. [Online]. Available: https://pubs.rsc.org/en/content/articlehtml/2015/md/c5md00057b.

[15] X. Chu, C. Wang, W. Wang, L. Liang, … W. L.-E. journal of, and undefined 2019, "Triazole derivatives and their antiplasmodial and antimalarial activities," Elsevier, Accessed: Jun. 02, 2020. [Online]. Available: https://www.sciencedirect.com/science/article/pii/S0223523419300595?casa_token=g6drY1VY-gsAAAAA:ELD77xX-5EoLXbjkb4qPDQd2DdHGUZ-zAPSVZXMYhaUuB_hr-Aritzfa13FcmjepqIdStCJD2JRo.

[16] W. Yan et al., "Design, synthesis, and antifungal activity of carboxamide derivatives possessing 1,2,3-triazole as potential succinate dehydrogenase inhibitors," Pestic. Biochem. Physiol., vol. 156, pp. 160–169, May 2019, doi: 10.1016/j.pestbp.2019.02.017.

[17] K. Lal and P. Yadav, "Recent Advancements in 1,4-Disubstituted 1H-1,2,3-Triazoles as Potential Anticancer Agents," Anticancer. Agents Med. Chem., vol. 18, no. 1, pp. 21–37, 2016, doi: 10.2174/1871520616666160811113531.

[19] Ding, C.; Zhang, Y.; Chen, H.; Wild, C.; Wang, T.; White, M.A.; Shen, Q.; Zhou, J. Overcoming synthetic challenges of oridonin A-ring structural diversification: Regio- and stereoselective installation of azides and 1,2,3-triazoles at the C-1, C-2, or C-3 position. Org. Lett. 2013, 15, 3718–3721.

[18] C. D. Hein, X. M. Liu, and D. Wang, "Click chemistry, a powerful tool for pharmaceutical sciences," Pharmaceutical Research, vol. 25, no. 10. NIH Public Access, pp. 2216–2230, Oct. 2008, doi: 10.1007/s11095-008-9616-1.

[19] X. Wang, B. Huang, X. Liu, and P. Zhan, "Discovery of bioactive molecules from CuAAC click-chemistry-based combinatorial libraries," Drug Discov. Today, vol. 21, no. 1, pp. 118–132, Jan. 2016, doi: 10.1016/j.drudis.2015.08.004.

[20] L. Liang and D. Astruc, "The copper(I)-catalyzed alkyne-azide cycloaddition (CuAAC) 'click' reaction and its applications. An overview," Coordination Chemistry Reviews, vol. 255, no. 23–24. Elsevier, pp. 2933–2945, Dec. 01, 2011, doi: 10.1016/j.ccr.2011.06.028.

[21] V. V. Rostovtsev, L. G. Green, V. V. Fokin, and K. B. Sharpless, "A Stepwise Huisgen Cycloaddition Process: Copper(I)-Catalyzed Regioselective 'Ligation' of Azides and Terminal Alkynes," Angew. Chemie Int. Ed., vol. 41, no. 14, pp. 2596–2599, Jul. 2002, doi: 10.1002/1521-3773(20020715)41:14<2596::AID-ANIE2596>3.0.CO;2-4.

[22] A. Oubella et al., "Diastereoselective synthesis and cytotoxic evaluation of new isoxazoles and pyrazoles with monoterpenic skeleton," J. Mol. Struct., vol. 1198, p. 126924, 2019, doi: 10.1016/j.molstruc.2019.126924.

[23] Zeroual, A.,Mazoir, N., Daran, J.-C., Akssira, M. & Benharref, A. " (4aS,10aS)-7-Hydroxy-8-isopropyl1,1,4a-trimethyl-1,2,3,4,4a,9,10,10aoctahydrophenanthrene: a new diterpenoid compound" (2008). Acta Cryst. E64, o604–o605.

[24] Oubabi, R., Auhmani, A., Ait Itto, M. Y., Auhmani, A. & Daran, J.-C. **“** (4b*S*,8a*S*)-1-Isopropyl-4b,8,8-trimethyl-4b,5,6,7,8,8a,9,10-octahydrophenanthren-2-yl acetate**,”**. (2014a). **Acta Cryst. E70, o317.**

[25] Oubabi, R., Auhmani, A., Ait Itto, M. Y., Auhmani, A. & Daran, J.-C. “ (4bS,8aS)-1-Isopropyl-4b,8,8-trimethyl4b,5,6,7,8,8a,9,10-octahydrophenanthren-2-yl benzoate“ (2014b). Acta Cryst. E70, o866-o867.

[26] D. J. McConkey, S. Orrenius, and M. Jondal, “Cellular signalling in programmed cell death (apoptosis),” Immunol. Today, vol. 11, no. C, pp. 120–121, 1990, doi: 10.1016/0167-5699(90)90048-E.

[27] S. Gupta, G. E. N. Kass, E. Szegezdi, and B. Joseph, “The mitochondrial death pathway: A promising therapeutic target in diseases,” J. Cell. Mol. Med., vol. 13, no. 6, pp. 1004–1033, 2009, doi: 10.1111/j.1582-4934.2009.00697.x.

[28] A. Zarei, A. R. Hajipour, L. Khazdooz, and H. Aghaei, “A fast and efficient method for the preparation of aryl azides using stable aryl diazonium silica sulfates under mild conditions,” Tetrahedron Lett., vol. 50, no. 31, pp. 4443–4445, Aug. 2009, doi: 10.1016/j.tetlet.2009.05.049.

[**29**] Bruker (2012). *APEX2*, *SAINT* and *SADABS*. Bruker AXS Inc., Madison, Wisconsin, USA.

[**30**] G. M. Sheldrick, SHELXT - Integrated space-group and crystal-structure determination. *Acta Crystallogr. Sect. A Found*. Crystallogr., 71 (2015), 3–8.

[**31**] G. M. Sheldrick, Crystal structure refinement with SHELXL. *Acta Crystallogr. Sect. C Struct. Chem*., 71 (2015), 3–8.

[**32**] K. Brandenburg . *DIAMOND*. Crystal Impact GbR, B *Bonn, Germany* (2006).

[**33**] M.A. Spackman, D. Jayatilaka, Hirshfeld surface analysis. CrystEngComm 11 (2009) 19–32

[**34**] J.J. McKinnon, D. Jayatilaka, M.A. Spackman. Towards quantitative analysis of intermolecular interactions with Hirshfeld surfaces. Chem. Commun. (2007) 3814–3816.

[**35**] M.J. Turner, J.J. McKinnon, S.K. Wolff, D.J. Grimwood, P.R. Spackman, D. Jayatilaka, M.A. Spackman, CrystalExplorer17, The University of Western Australia, 2017.

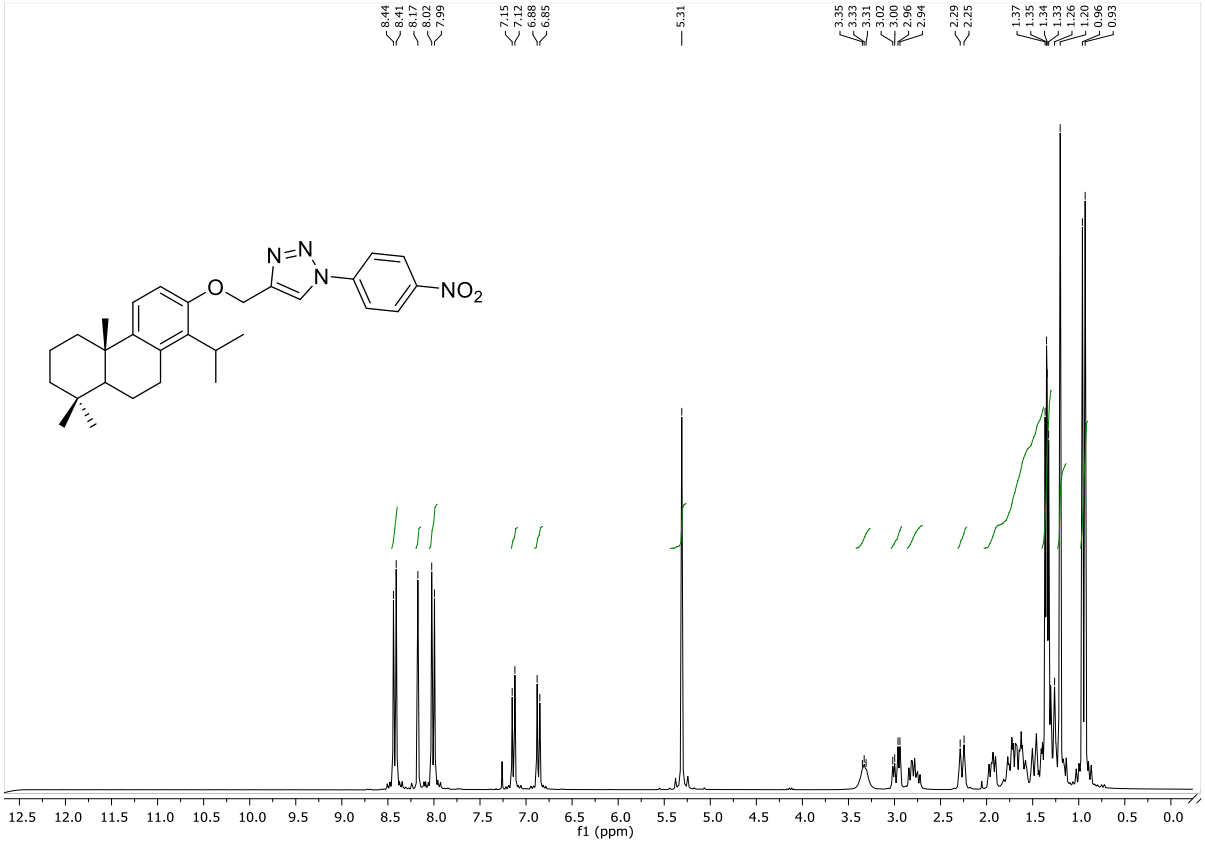
8.44
8.41
8.17
8.02
7.99
7.15
7.12
6.88
6.85
5.31
3.35
3.33
3.31
3.02
3.00
2.96
2.94
2.29
2.25
1.37
1.35
1.34
1.33
1.26
1.20
0.96
0.93
N=N
N
O
NO2
f1 (ppm)

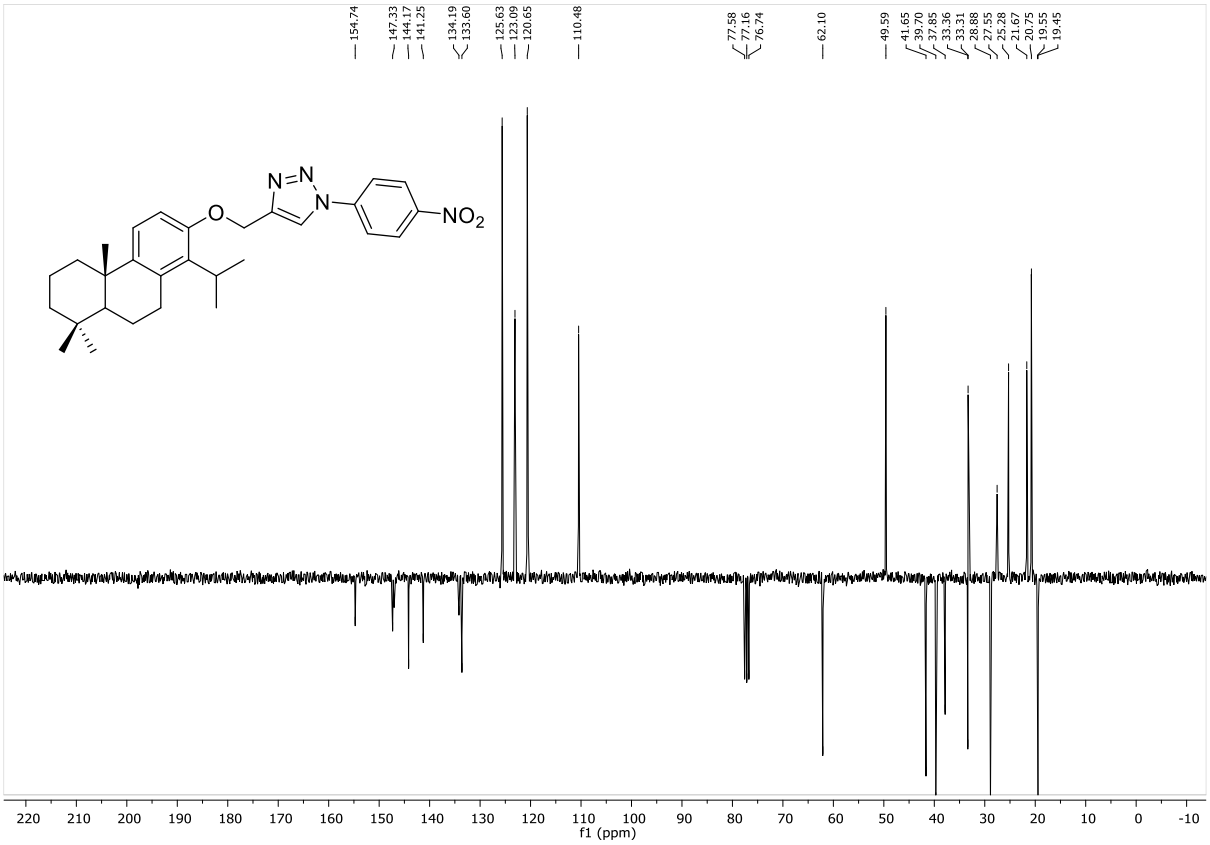
154.74
147.33
144.17
141.25
134.19
133.60
125.63
123.09
120.65
110.48
77.58
77.16
76.74
62.10
49.59
41.65
39.70
37.85
33.36
33.31
28.88
27.55
25.28
21.67
20.75
19.55
19.45
N=N
N
O
NO2
f1 (ppm)